

# Development of a time correction algorithm for a precise synchronization of a free running Rubidium clock with the GPS Time

Claire Dalmazzone <sup>1,†,\*</sup> , Mathieu Guigue <sup>1,†</sup> , Lucile Mellet <sup>1,2,†</sup> , Boris Popov <sup>1,†</sup> , Stefano Russo <sup>1,†</sup> and Vincent Voisin <sup>1,†</sup>

<sup>1</sup> Laboratoire de Physique Nucléaire et de Hautes Energies (LPNHE), Sorbonne Université, CNRS/IN2P3, Paris, France

<sup>2</sup> Michigan State University, Department of Physics and Astronomy, East Lansing, Michigan, USA; melletl1@msu.edu

\* Correspondence: [claire.dalmazzone@lpnhe.in2p3.fr](mailto:claire.dalmazzone@lpnhe.in2p3.fr)

† These authors contributed equally to this work.

**Abstract:** We present results of our study devoted to development of a time correction algorithm needed to precisely synchronize a free running Rubidium clock with the Universal Time Coordinated (UTC). This R&D is performed in view of the Hyper-Kamiokande (HK) [1] experiment currently under construction in Japan, which requires a synchronization with UTC and between its different experimental sites with a precision better than 100 ns. We use a Global Navigation Satellite System (GNSS) receiver to compare a PPS and a 10 MHz signal, generated by a free running Rubidium clock, to the Global Positioning System (GPS) Time signal and to correct the Rubidium signal. We fit the Rubidium - GPS time residuals data with polynomials functions of time over a certain integration time window to extract a correction of the free running Rubidium signal in offline or online mode. In online mode, the latest fits results are used to correct the Rubidium signal until a new comparison to GPS becomes available. We show that with an integration time window of timing data residuals of around  $10^4$  seconds, we can correct the free running Rubidium signal for the frequency random walk noise so that the timing residuals stay within a  $\pm 5$  ns range in both offline or online correction mode.

**Keywords:** precise timing; atomic clock; Rb; PHM; GPS; GNSS; UTC

## 1. Introduction

A precise synchronization of a free running atomic clock signal with the Universal Time Coordinated (UTC) or with another signal is a necessity in many applications, particularly in physics experiments including several experimental sites that must be synchronized. A good example is long baseline neutrino oscillation experiments, like OPERA [2] (2006-2012), T2K [3] (from 2010) and NOvA [4] (from 2014), where a beam of neutrinos is produced and characterized in a first experimental site and detected, after several hundreds of kilometers of propagation, at another site to measure a change of the beam properties. Several next generation long baseline neutrino experiments are being built at the moment, like Hyper-Kamiokande (HK) [1] that plans to start taking data in 2027 and DUNE [5] that should begin sometime after 2029. These experiments require a synchronization between the different experimental sites. For HK for instance, this requirement is of 100 ns or better. Moreover, multi-messenger programs that plan to compare different components of astrophysical events [6] (e.g.: gamma-ray bursts, gravitational waves, neutrino emissions of supernovae, etc.) require a synchronization with UTC of different experiments located all over the world. For instance, to enter the SuperNova Early Warning System (SNEWS) network [7], a synchronization to UTC better than 100 ns is needed.

Many physics experiments use atomic oscillators as frequency references because of their good short term stability. One of the reference oscillators available are Rubidium

**Citation:** Dalmazzone, C.; Guigue, M.; Mellet, L.; Popov, B.; Russo, S.; Voisin, V. Title. *Journal Not Specified* **2024**, *1*, 0. <https://doi.org/>

Received:

Revised:

Accepted:

Published:

**Copyright:** © 2024 by the authors. Submitted to *Journal Not Specified* for possible open access publication under the terms and conditions of the Creative Commons Attribution (CC BY) license (<https://creativecommons.org/licenses/by/4.0/>).

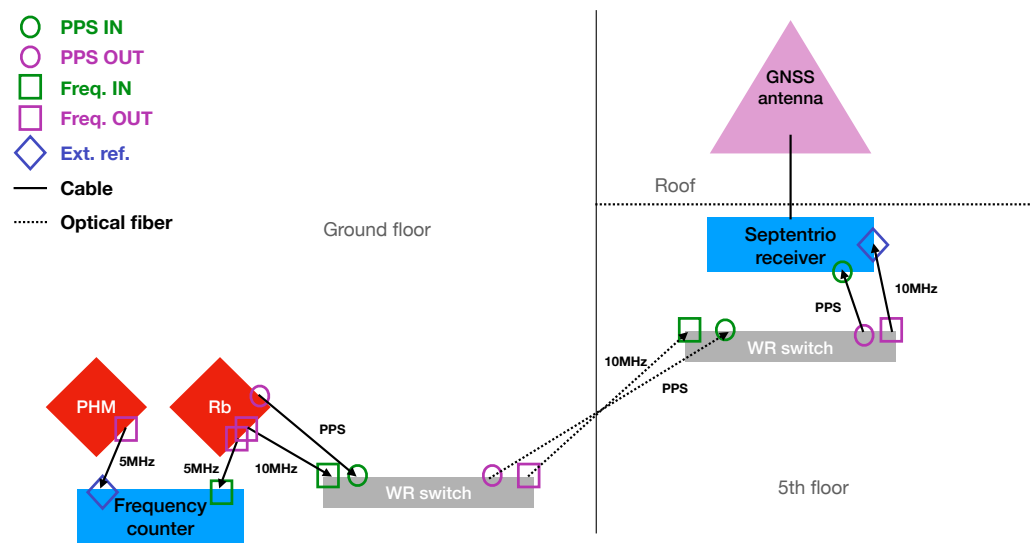


**Figure 1.** Experimental setup used in this work. Part of the equipment is installed at the ground floor and the other part at the fifth floor. The relevant signals generated at the ground floor are transported to the fifth floor via optical fibers with the White Rabbit (WR) protocol. This particular setup mimics what could happen in underground experiments where the clock signal would be generated underground whereas the GPS antenna and receiver would be above-ground.

clocks, which are generally chosen for affordability as it was the case for the T2K [8] and Super-Kamiokande [9] timing systems. However, Rubidium clocks signals usually drift away from a stable reference because of frequency drift and random walk. For synchronization to UTC, this drift usually needs to be prevented or corrected. A common solution is to discipline the average frequency of the clock to the signals of an external Global Navigation Satellite System (GNSS) receiver, with a chosen integration time window long enough in order not to deteriorate the short term stability of the clock. However, it presents some drawbacks like the fact that the user has little control on the setup. In case of problems (like jumps in the time signal), it is difficult to understand where they come from (GPS Time, receiver, the master clock, etc.) and to assess the uncertainty on the synchronization to UTC. The R&D work presented in this paper and introduced in [10] is focused on designing and characterizing an alternative method that allows more freedom to the user and a better understanding of the process. It is based on known metrology techniques [11,12]. The proposed method uses a free running atomic clock to derive a time signal that is corrected in post-processing using comparisons to GNSS Time. Let us note that the GNSS time is a good approximation of the UTC, within a few nanoseconds. In that way, we can safeguard all the information (the raw signal, the comparisons to GPS Time, the derived correction etc.) and apply the correction in either online (during the data-acquisition) or offline modes.

## 2. Materials and Methods

### 2.1. Experimental setup

The experimental setup that we used is schematized in Figure 1. It is located at the Pierre and Marie Curie (Jussieu) campus of the Sorbonne University in Paris. The setup consists of two main parts: one represents the timing generation and correction setup, that could be reproduced in physics experiments, and the second part is related to testing the efficiency of the correction method. In the first part a Rubidium clock (Rb) in free running mode, at the ground floor of the laboratory, generates a Pulse Per Second (PPS) and a 10 MHz signal that are transported to the fifth floor with the White Rabbit (WR) protocol. The 10 MHz signal is used by a GPS receiver as a reference for its internal clock. The

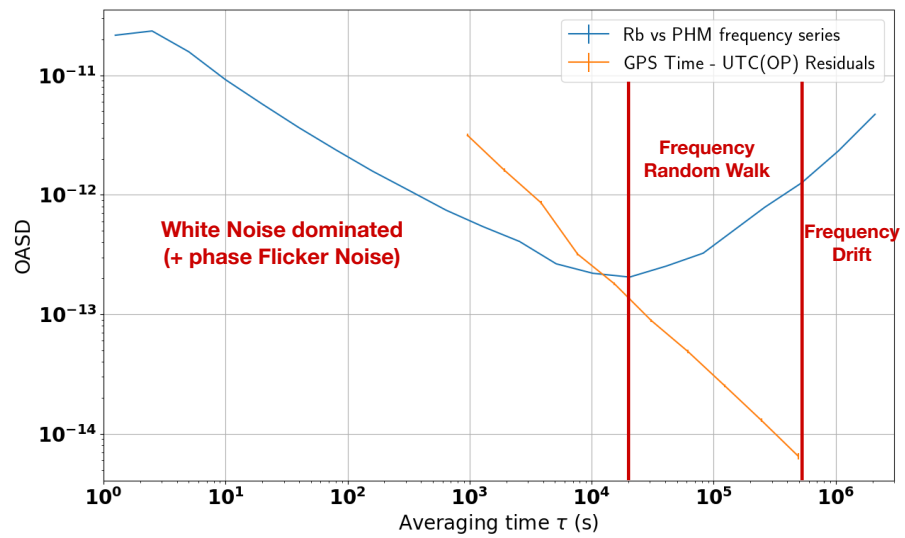


**Figure 2.** Overlapping Allan Standard Deviation of the Rb/PHM frequency ratio series (in blue), measured by the frequency counter before any correction, and of GPS Time vs UTC(OP) (in orange) measured by the Septentrio receiver. The main type of noises affecting the Rubidium clock stability are indicated where they are limiting the stability.

receiver is used to measure comparisons between the GPS satellites signals provided by the antenna on the roof (above the fifth floor) and the Rubidium clock time signal. This physical distance between the time generation part and the receiver was done on purpose to mimic what would happen in many physics experiments. Indeed, in Hyper-Kamiokande, the Rubidium clock would be placed inside a mountain where a cavern has been dug to host the detector whereas the receiver would have to be placed outside in a valley. The second part of our experimental setup is contained in the experimental room at the ground floor and its purpose is to validate the performance of the method, it would not be reproduced in the final setup in Hyper-Kamiokande. It consists in a frequency counter measuring the frequency of the 5 MHz signal generated by the Rubidium clock. The reference for the internal clock of the counter is an external 5 MHz signal generated by a Passive Hydrogen Maser (PHM).

### 2.1.1. Rubidium clock

The Rubidium clock used is the FS725 Rubidium Frequency Standard sold by [Stanford Research Systems](#) integrating a rubidium oscillator of the PRS10 model. It provides two 10 MHz and one 5 MHz signals with low phase white noise and the stability measured via the Allan Standard Deviation (ASD) [13] at 1 s of  $\sim 2 \times 10^{-11}$  (see Figure 2). It also provides a PPS output with a jitter of less than 1 ns. Its 20 years aging was estimated to less than  $5 \times 10^{-9}$  and the Mean Time Before Failure is over 200,000 hours. It can also be frequency disciplined using an external 1 PPS reference, like the GPS for instance. The FS725 is installed at the ground floor of our laboratory and its 10 MHz and 1 PPS output are transported to the GPS receiver at the fifth floor.

### 2.1.2. White Rabbit switches

The White Rabbit (WR) project [14] is a collaborative effort involving CERN, the GSI Helmholtz Centre for Heavy Ion Research, and other partners from academia and industry. Its primary objective is to develop a highly deterministic Ethernet-based network capable of achieving sub-nanosecond accuracy in time transfer. Initially, this network was implemented for distributing timing signals for control and data acquisition purposes at CERN's accelerator sites.

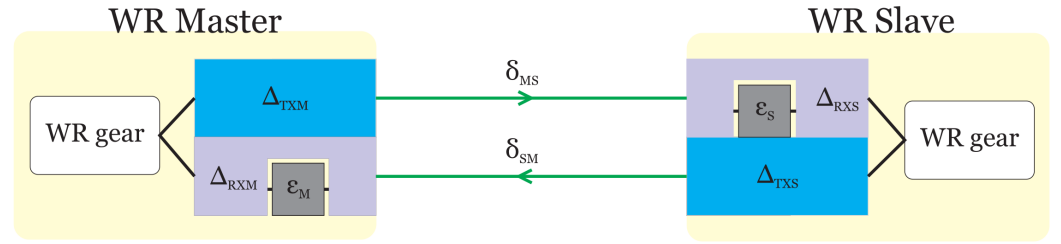


**Figure 3.** White Rabbit link model, from [15]

The experimental setup described uses two WR switches to propagate the Rubidium clock PPS and frequency signals from the ground floor to the fifth floor with great precision. 92

### Calibration 93

In order to achieve a sub-nanosecond synchronization between switches a calibration of the link must be done. A White Rabbit link between two devices is characterized by specific hardware delays and fiber propagation latencies. 94

Each WR Master and WR Slave possesses fixed transmission and reception delays ( $\Delta T_{XM}$ ,  $\Delta RXM$ ,  $\Delta T_{XS}$ ,  $\Delta RXS$ ). These delays are the cumulative result of various factors such as SFP transceiver, PCB trace, electronic component delays, and internal FPGA chip delays. Additionally, there is a reception delay on both ends caused by aligning the recovered clock signal to the inter-symbol boundaries of the data stream, referred to as the bitslide value ( $\epsilon_M$  and  $\epsilon_S$  in Figure 3). 95

We can see the results of calibration process using a counter in Figure 4, the difference of PPS signals between the WR slave and master switches changes from 165 ps to 60 ps (with a 100 m fiber). Delays introduced by the cables used was subtracted to the mean values. 96

### REFIMEVE 97

Note that the LPNHE, as a part of the T-REFIMEVE network [16,17], has access through a dedicated switch to the official French realization of the UTC, called UTC(OP) (for Observatoire de Paris) [29], transported from the SYRTE laboratory via White Rabbit protocol. REFIMEVE is a French national research infrastructure aiming at the dissemination of highly accurate and stable time and frequency references to more than 30 research laboratories and research infrastructures all over France. The reference signals originate from LNE-SYRTE and are mainly transported over the optical fiber backbone of RENATER, the French National Research and Education Network. The UTC(OP) signal was not used in the final experimental setup because we do not foresee to have access to such a high precision signal in HK experiment **It was however used to characterize the GPS time signal measured by the Septentrio receiver and whose OASD is shown in Figure 2.** 98

#### 2.1.3. Septentrio GPS antenna and receiver 99

We use the **Septentrio PolaNt Choke ring GNSS antenna** that supports GNSS signals from many satellite constellations including GPS, GLONASS, Galileo, BeiDou and others. In this work, we restrict the analysis to GPS but it can easily be generalized to any subset of constellations. The antenna position has been previously measured to a precision better than 6 mm by trilateration with the help of a web-based service provided by Canadian government [26]. We use a **Septentrio PolaRx5 GNSS reference receiver** as a timing receiver to compare GPS Time to the Rubidium. The receiver performs measurements based on the 10 MHz reference signal coming via White Rabbit from the Rubidium clock. The Rubidium clock 1 PPS signal is also transported to the receiver via White Rabbit to allow, at initialization, to identify the 10 MHz cycle. Note that this 1 PPS input is kept during the whole data-taking to avoid possible phase jumps due to perturbations. The Septentrio receiver provides one measurement every 16 min which is the middle point of the linear 100

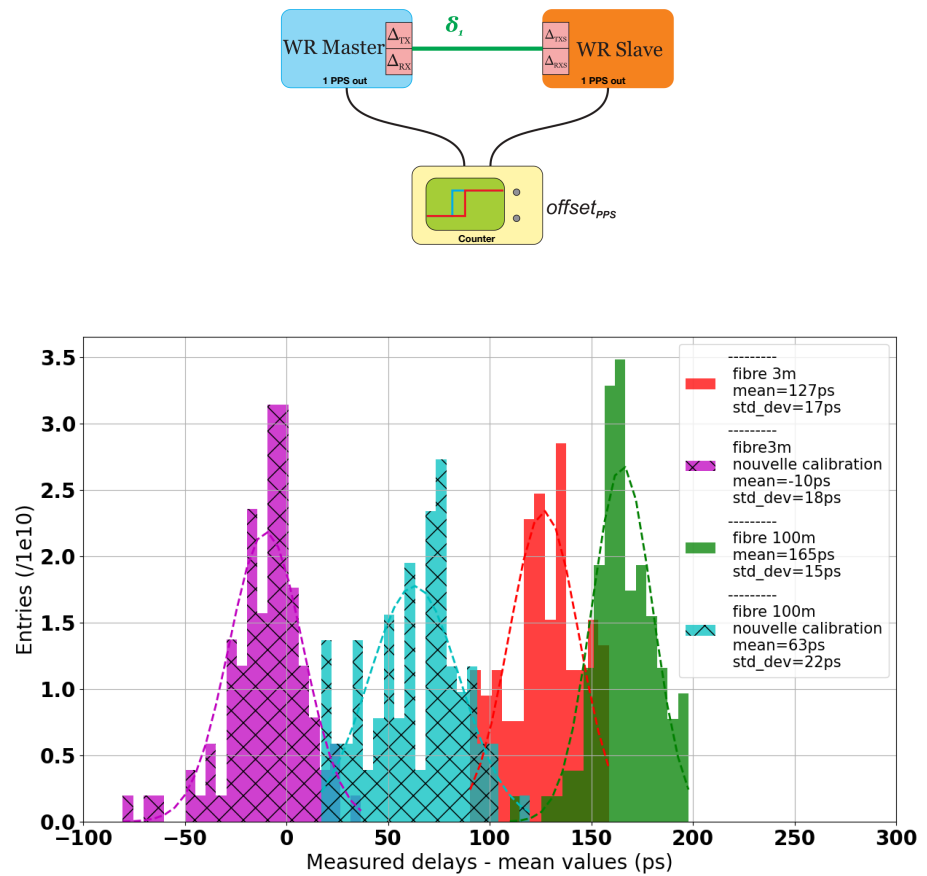


**Figure 4.** Difference between the PPS OUT signals of the White Rabbit slave and master switches before and after calibration

function fitted from the 13 min of data from the beginning of this 16 min time window. The results of the measurements are registered using the CCGTTS file format [18].

Before taking measurements, the whole system has been calibrated against official reference signals from the SYRTE laboratory. As it can be seen in Figure 5, the following delays need to be measured and taken into account during operation [20]. The calibration procedure [30] consists in measuring these:

- $\chi_S$ : internal delay inside the antenna, frequency dependent
- $\chi_C$ : delay caused by the antenna cable
- $\chi_R$ : internal delay of the receiver for the antenna signal, frequency dependent
- $\chi_P$ : in case an external signal is given in input, connection cable delay
- $\chi_O$ : in case an external signal is given in input, internal receiver delay between external 1 PPS and internal clock

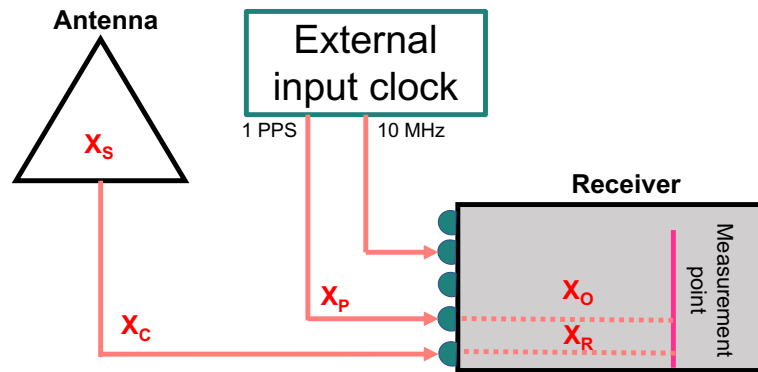


**Figure 5.** Delays to consider for the selected GNSS receiver+antenna pair, from [19]

$X_S$  and  $X_R$  depend on the GPS frequency that is being read, meaning it is specific to each frequency of each GPS constellation. The calibration was performed for both GPS and Galileo constellations, each having two available frequencies. The cable delays  $X_C$  and  $X_P$  were evaluated with an oscilloscope by sending a pulse in the cable and measuring the timing of the reflection. To reproduce the experimental conditions of underground experiments like HK or DUNE where the GPS antenna is outside, away from the detector, a 100 m cable was used and calibrated. The total cable delay was measured to be 505 ns. The internal delays of the antenna and receiver can only be measured together (for each frequency) as  $INTDLY = X_S + X_R$ . This was done through a comparison with OP73, one of the calibrated receivers of SYRTE, and with UTC(OP), the French realization of UTC, as an input to the two receivers. The values of INTDLY found for the two most widely available frequencies of the GPS constellation (L1 and L2) and the Galileo constellation (E1 and E5a) are given in Table 1.

**Table 1.** Values of INTDLY in ns found for the first antenna+receiver system calibrated at the SYRTE lab against the OP73 station

GPS L1	GPS L2	Galileo E1	Galileo E5a
25.832	22.871	28.242	25.431

The delays  $X_C$ , INTDLY, and REFDLY can then be given as parameters of the receiver so that they are automatically handled in any further use of the receiver. Uncertainty on the measured delays were evaluated to 4 ns according to estimations fixed for the employed method. The calibration needs to be re-done for any new antenna+receiver+antenna cable combination.

#### 2.1.4. Passive Hydrogen Maser

A Passive Hydrogen Maser (PHM) from T4 Science was also acquired. Note that this instrument is not available anymore. This atomic clock is approximately 10 times more expensive than a Rubidium clock but is also much more stable. Indeed, the Allan Standard Deviation (ASD), measured with our PHM in April 2022, was only of  $\sim 3 \times 10^{-13}$  at 1 s and of  $1.5 \times 10^{-15}$  at 1 day. The PHM provides a 1 PPS signal as well as two outputs of 5 MHz, two outputs of 10 MHz, one output of 100 MHz and a sine output of 1 MHz as well as a 2.048 MHz square signal. Here, we use the PHM to generate a "perfect signal" to compare our Rubidium clock to.

#### 2.1.5. Frequency counter

The frequency counter is the 53220A model from Keysight Technologies. It has two input channels and an input for an external frequency to use as a reference for its internal

clock. The instrument can be used to measure the frequency of a signal input at any of the two channels. The instrument either uses directly its internal oscillator or, if specified by the user, the internal oscillator can be tuned to the external reference frequency. The external reference must be a sine wave with a frequency of 1, 5 or 10 MHz. The measurement resolution depends on the gate time corresponding to the integration time window: the longer the gate time, the better the resolution. The default resolution corresponds to a 0.1 s gate time.

The frequency counter was used in continuous mode to measure the Rubidium clock 5 MHz signal frequency simultaneously to the measurements performed by the Septentrio receiver. The external frequency reference was set to be the 5 MHz signal of the PHM and the resolution was set to 0.01 mHz which corresponds to a relative resolution of  $2 \times 10^{-11}$ . This resolution is good enough to measure the ASD of the Rubidium clock at low averaging times.

## 2.2. Corrections methods

### 2.2.1. General principle

To synchronize our clock signal to UTC, we apply a time-dependent correction (quadratic or linear) to the signal generated by the free running Rubidium clock  $\phi_{Rb}(t)$ . We model the  $k^{\text{th}}$  portion of the time series ( $dt_{Rb,GPS}$ ), defined as the difference between the free running Rb clock and the GPS Time, as a (one or two degrees) polynomial of time

$$\forall t \in [t_{k-1}, t_k], dt_{Rb,GPS}(t) = a_k \cdot t^2 + b_k \cdot t + c_k. \quad (1)$$

The coefficients  $a_k$  ( $a_k = 0$  in case of linear fit),  $b_k$  and  $c_k$  of the polynomials are extracted from least square polynomial fits of the time difference distributions. The fits of these residuals, obtained from the Septentrio receiver, are performed for every  $k^{\text{th}}$  time window of length  $\Delta t$ . In other words, we model the Septentrio measurements with a piece-wise polynomial function of time. For the  $k^{\text{th}}$  time window (between  $t_k$  and  $t_{k+1}$ ), we get the corrected time signal

$$\forall t \in [t_k, t_{k+1}], \phi_{Rb,corr}(t) = \phi_{Rb}(t) - a_k \times t^2 - b_k \times t - c_k. \quad (2)$$

The time-length  $\Delta t$  of the pieces (time windows) has to be chosen carefully. In particular, it should be short enough in order to correct for the effect of the frequency random walk of the Rubidium clock but not too short to not deteriorate its good short term stability.

In the following, we consider two types of correction: the offline and the online corrections. The difference between the two methods is illustrated in Figure 6. The offline correction consists in using the Septentrio data from the same time-window as the Rubidium signal we want to correct to extract the  $a_k$ ,  $b_k$  and  $c_k$  coefficients. This correction is called offline because it requires the Septentrio data from up to  $t_k + \Delta t = t_{k+1}$  to correct all the Rb signal between  $t_k$  and  $t_{k+1}$  so it cannot be performed in real-time (because one would need to wait a time  $\Delta t$  to extract the correction coefficients for the signal at time  $t_k$ ).

The online correction consists in correcting the Rubidium signal between  $t_k$  and  $t_{k+1}$  using Septentrio data collected before  $t_k$ . One example of online correction is illustrated in Figure 6 where Septentrio data received between  $t_{k-1} = t_k - \Delta t$  and  $t_k$  are used to correct the Rubidium signal between  $t_k$  and  $t_{k+1} = t_k + \Delta t$ . This method is called online because it can be applied in real time. In the following, we will consider the most frequent possible update of the  $a_k$ ,  $b_k$  and  $c_k$  coefficients: they will be updated every time we receive a new data point from the Septentrio receiver (every  $\delta t \approx 16$  minutes in our case). This means that we have  $t_{k+1} = t_k + \delta t$  so that the  $a_k$ ,  $b_k$  and  $c_k$  coefficients are extracted using Septentrio data between  $t_k - \Delta t$  and  $t_k$  and are used to correct the Rubidium signal between  $t_k$  and  $t_k + \delta t$ . In that particular case every Septentrio data point will have been used in multiple fits, the number depending on the length of the fit time window  $\Delta t$ .

The performance of the correction is evaluated in two ways. First, we look at the stability of the corrected free running Rubidium signal estimated with the Overlapping

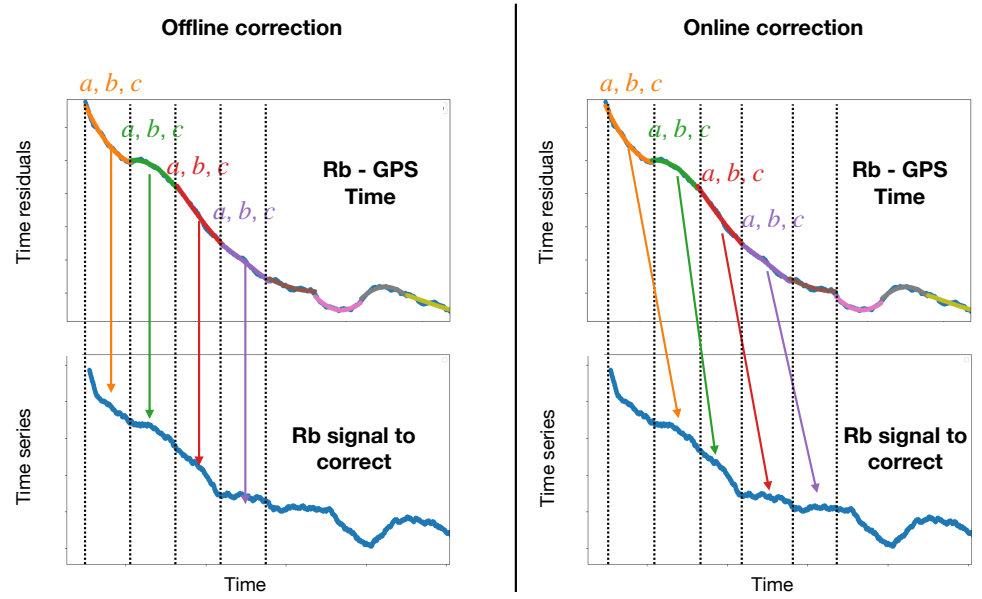


**Figure 6.** Schematic representation of the offline (left) and online (right) corrections. In the offline correction, we extract the correction coefficients using Rubidium - GPS Time comparison from the same time-window as the data we want to correct. In the online correction, we use Rubidium - GPS Time comparison from the previous time-window with respect to the data interval we want to correct. Only the second correction can be applied in real time as it only requires comparisons with GPS from the past of the signal we correct.

Allan Standard Deviation (OASD). Then, we also look at the time residuals against GPS signal after correction. 224  
225

### 2.2.2. Validation of the method with simulations 226

Before evaluating the performance of our timing system when integrating the correction algorithm, the method was validated on simulated signals [19] in order to isolate the effect and performance of the correction from any measurement effect. 227  
228  
229

#### Simulation details 230

Three types of signals were considered: a perfect PPS to use as a reference to evaluate the performance, a free Rubidium clock and a GPS time signal, as measured by the Septentrio receiver. Phase series were simulated and transformed into PPS time series for simplicity. The quadratic drift was not included because it is deterministic and therefore does not require further study for being corrected. At first order, the clock signal can be modeled by white noise (WN) in both phase and frequency as well as a random walk (RW) noise in frequency. Based on the characterization of the Rb clock, the phase and frequency flicker noises can be neglected for this purpose. Indeed, the characterization of our Rubidium clock in Figure 2 showed that the frequency flicker noise had a negligible impact on the ASD. Furthermore, the phase white n and flicker noises have a similar impact on the standard ASD and cannot be distinguished here. We chose to ignore the phase flicker noise as it is less straightforward to simulate and it should not impact the long term random walk that we want to correct. The GPS Time can be modeled as pure phase white noise. The corresponding OASD as a function of the averaging time  $\tau$  can be modeled [21–23] by: 231  
232  
233  
234  
235  
236  
237  
238  
239  
240  
241  
242  
243  
244  
245

$$OASD(\tau) \cong A_{WNp} \times \tau^{-1} + A_{WNf} \times \tau^{-1/2} + A_{RWf} \times \tau^{+1/2}. \quad (3)$$



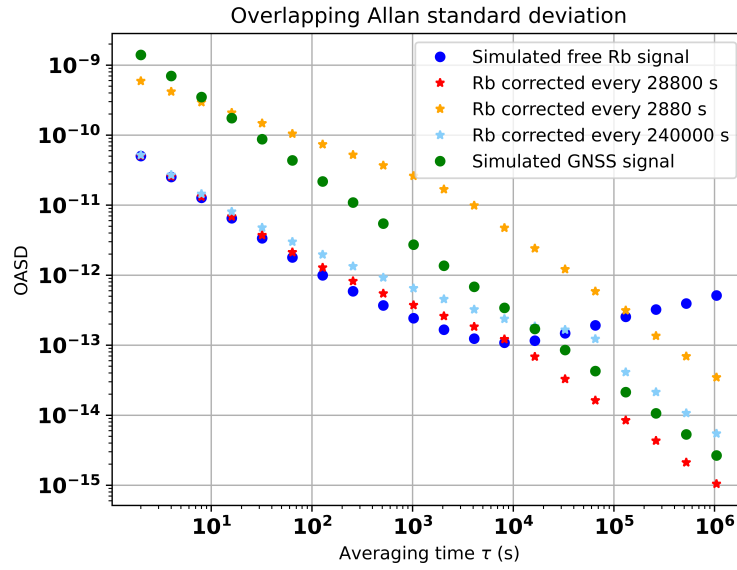


**Figure 7.** Comparison of overlapping ASD for corrected signals with different time windows

The amplitudes  $A$  of these main frequency and phase noises were determined through fitting this model (Eq. 3) to the OASD of the data when characterizing our equipment (see Figure 2) and found to be:

$$\begin{aligned} A_{WNf} &= 7 \times 10^{-12} \text{ s}^{1/2}, \\ A_{RWf} &= 1 \times 10^{-15} \text{ s}^{-1/2}, \\ A_{WNP} &= 5 \times 10^{-11} \text{ s}, \end{aligned} \quad (4)$$

for the free Rb clock and for the GPS Time:

$$\begin{aligned} A_{WNf} &= 0 \text{ s}^{1/2}, \\ A_{RWf} &= 0 \text{ s}^{-1/2}, \\ A_{WNP} &= 2 \times 10^{-9} \text{ s}, \end{aligned} \quad (5)$$

with indices  $f$  and  $p$  for frequency and phase respectively.

The equivalent of  $10^6$  s of data was simulated. To mimic the output of the GPS receiver, time differences between the simulated Rubidium clock and the simulated GPS Time ( $\Delta t_{Rb-ref}^i$ ) are computed every 16 mn.

### Offline corrections

First, the offline corrections were tested on the simulated data. In Figure 7, the uncorrected simulated signals of the GPS and the clock are reported in dotted symbols for comparison. The increase of the clock's OASD after  $\tau = 10^4$  s due to the random walk is clearly visible. One can see that the OASD of the corrected signals (starred symbols) do eliminate the random walk at longer terms which indicates a success of the correction method. Moreover, one can determine that the ideal length  $\Delta t$  of the correction time windows lies around  $3 \times 10^4$  s which corresponds logically to the intersection of the free Rb clock and GPS Time OASD curves. Indeed, the red curve with a time window of 28800 s shows an ideal combination of the short-term stability of the clock and the absence of random walk at longer scales. On the opposite, the yellow (shorter time window) and light blue (longer time window) curves show respectively a degradation of the short term performance and a remaining random walk component in the region between  $\tau = 10^4$  s and the time window length (here 240000 s).

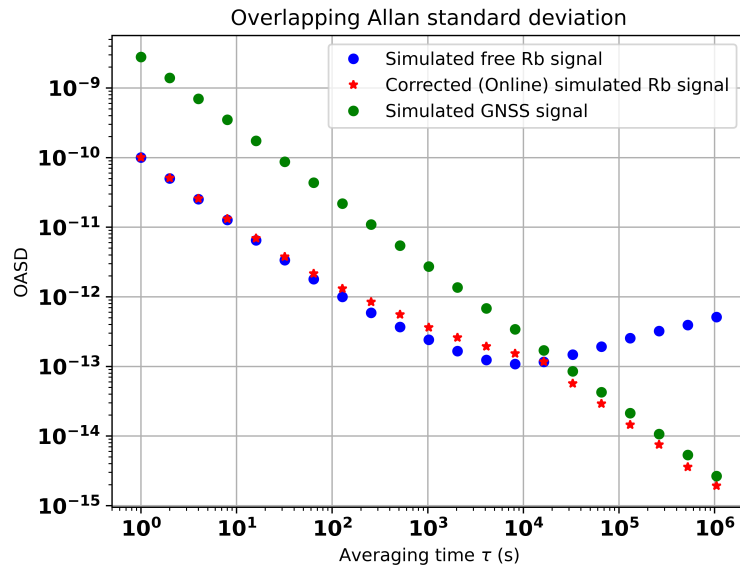


**Figure 8.** After online corrections at  $3 \times 10^4$  s: Overlapping ASD with respect to perfect signal

### Online corrections

The online correction method was then applied to the simulated data using time series directly and a correction window length of  $\Delta t = 3 \times 10^4$  s. The results are shown in Figure 8 in red and prove to be just as efficient as the offline correction method to remove the random walk at longer time scales which is the main goal. The overall precision on the long term region (after  $\approx 10^3$  s) is as expected slightly degraded compared to the offline correction.

### Conclusion on simulation

As a conclusion, it can be said that the application of the correction algorithms to the simulated signals allowed us to validate the chosen correction methods, both the offline and online ones. Indeed, looking at the residuals after correction in Figure 9, one can see that the remaining variations for both methods are well within the experiment's requirements as they stay within a few ns. Seven different simulations were produced to take into account statistical fluctuations and the remaining time variations were found to be for offline and online corrections respectively  $\sigma_{Off} = 0.64 \pm 0.06$  ns and  $\sigma_{On} = 1.15 \pm 0.07$  ns. Finally, it is important to note that although this validates the methods for application on data, those are simplified simulations, in particular because only the main noise types are taken into account. As a result, we do expect differences of performance of the correction on data. It is also possible that the optimal time window for the correction is slightly different for data because the simulations are not exact representation of data. Two main differences can be noted: the absence of frequency drift and flicker noises in the simulated Rubidium signal and the fact that we assume a perfect signal to compare the Rubidium signal too when evaluating the OASD.

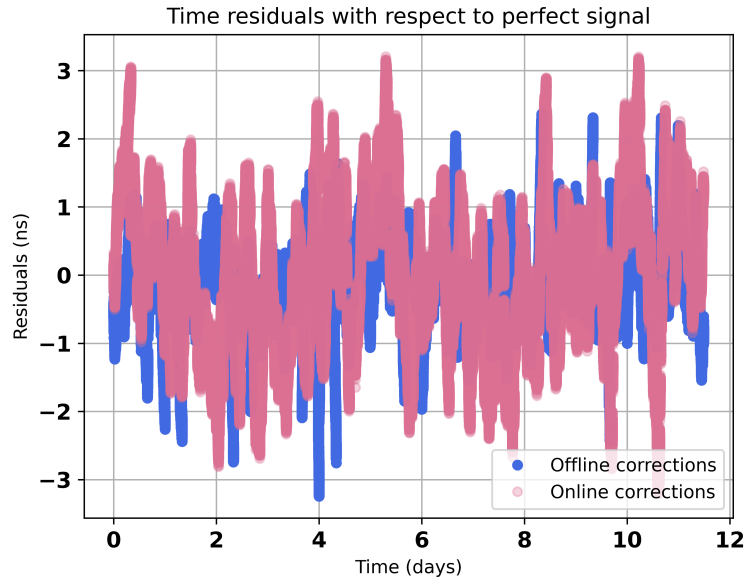


**Figure 9.** Comparison of time variations for simulated signals corrected with the offline method (blue) or with the sliding interval online method (pink)

### 2.2.3. Implementation on data

To check the impact of the correction on the Rubidium clock, we compare the free running and corrected signal to another more stable clock, like a Passive Hydrogen Maser. The PHM signal plays the role of the perfect signal used for the simulations, while obviously not being perfect. This first difference is to take into account while comparing performances on simulated data to performance on experimental data. In the following, we will also quantify the stability of the Rubidium signal using the OASD of a series of frequency ratios<sup>1</sup> between this signal and the 5 MHz generated by the PHM. Measuring this ratio frequently, like once per second, would allow to also evaluate the very short term stability of the corrected signal which is not possible with the Septentrio measurements that are integrated over 16 minutes. We used the frequency counter to provide every second a measurement of the Rubidium clock 5 MHz frequency  $f_{Rb}^i$  taking the PHM 5 MHz generated signal as a frequency reference  $f_{ref}$ . We then performed a simultaneous correction of the the Rubidium - GPS Time, as measured by the Septentrio receiver, and of this frequency ratio  $f^i = f_{Rb} / f_{ref}$  series. Comparing the OASD of the corrected frequency series to the uncorrected one, one can quantify the short term stability after correction while making sure that the random walk was corrected. We can also use this comparison to optimize the value of  $\Delta t$  in order to achieve the lowest Allan Standard Deviation possible at all averaging time windows.

## 3. Results

In this Section, we present the results of the correction of the Rubidium time signal obtained for simultaneous measurements of  $\sim 50$  days with the Septentrio receiver and the frequency counter with PHM 5 MHz signal as a frequency reference. The frequency measurements are divided by the expected value to obtain a series of Rb/PHM frequency ratios. The OASD of such a frequency series is shown in Figure 2. Note that the statistical uncertainties on the estimated OASD, due to the limited number of samples per averaging time, are included as error bars for both curves (Rb and GPS) but they are too small to be visible. Indeed for the Rb vs PHM OASD, the statistical uncertainty is at the permil level. Up to an averaging time of around  $10^4$  s, the stability is limited only by the phase and then the frequency white noise. After that, the OASD first increases as  $\tau^{1/2}$  which

<sup>1</sup> according to equation (10) of [24]

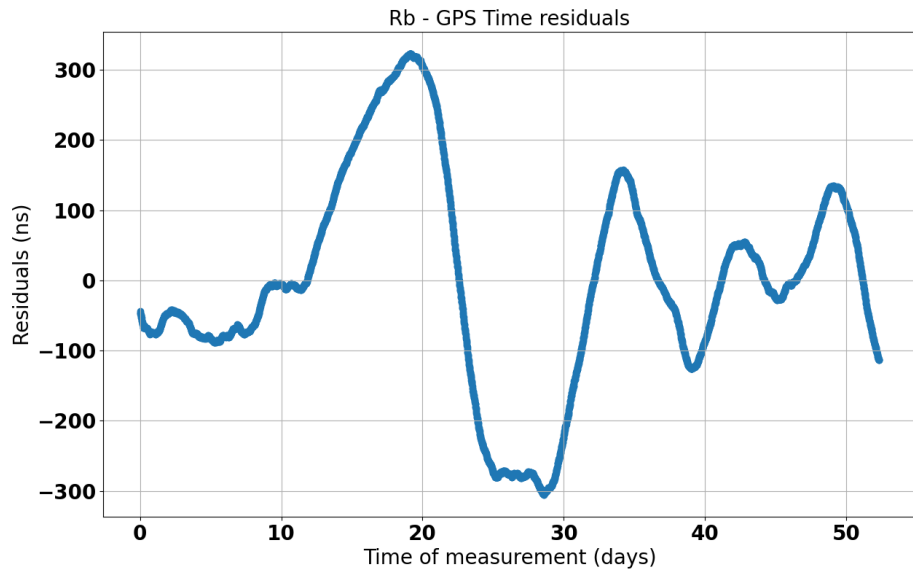


**Figure 10.** Time distribution of the time residuals between the Rubidium clock and GPS Time as measured by the Septentrio receiver. The distribution is already corrected for the deterministic drift of the Rubidium clock. The large time scale variations are caused by the frequency random walk of the Rubidium clock.

is characteristic of the frequency random walk. From  $\tau \approx 5 \times 10^5$  s, the OASD increases proportionally to  $\tau$ . This is characteristic of a deterministic frequency drift which can be easily characterized and corrected contrary to the frequency random walk. In comparison, the OASD of the difference between GPS Time and UTC(OP) that we receive from the SYRTE laboratory via White Rabbit, is only limited by a white noise at least up to an averaging time of  $5 \times 10^5$  s: the OASD keeps decreasing with the averaging time. At low averaging times, the GPS stability is worse than the Rb because of this white noise: the GPS OASD is of around  $3 \times 10^{-12}$  at 960 s compared to around  $7 \times 10^{-13}$  OASD for the Rubidium clock. However, at around  $10^4$  s, the stability of the Rb signal becomes worse compared to GPS Time because of the frequency random walk and drift of the Rubidium clock.

In this paper, we used only the GPS satellites with an elevation angle (angle between line of sight and horizontal direction) superior to  $15^\circ$  to extract the Rubidium time residuals distribution. During the whole data-taking period, for each data point, the Septentrio receiver picked up an average of 6.5 GPS satellites and at least 4 GPS satellites for each data point. To obtain the Rubidium vs GPS Time residuals, we take the mean value of the PPS differences between the Rubidium clock and each GPS satellite picked up in the same integration time window of the Septentrio receiver. The obtained time residuals is shown in Figure 10. The time residuals shown here have already been corrected for the deterministic drift discussed before as this can be easily monitored and corrected for contrarily to the random walk. The correction coefficients will be extracted from this time residuals distribution. Before correction, we see that after a few days of data-taking, the Rb clock can drift away from the GPS Time by more than a hundred nanoseconds because of the random walk noise, hence the need for a correction.

### 3.1. Offline correction

Figure 11 shows the Allan standard deviation of the Rubidium/PHM frequency ratios measurements. Note that a relative resolution of  $10^{-11}$  was chosen for the frequency measurement with the frequency counter. This is very close to the Phase White Noise of the free running Rubidium so it does not impact significantly the Allan Standard Deviation

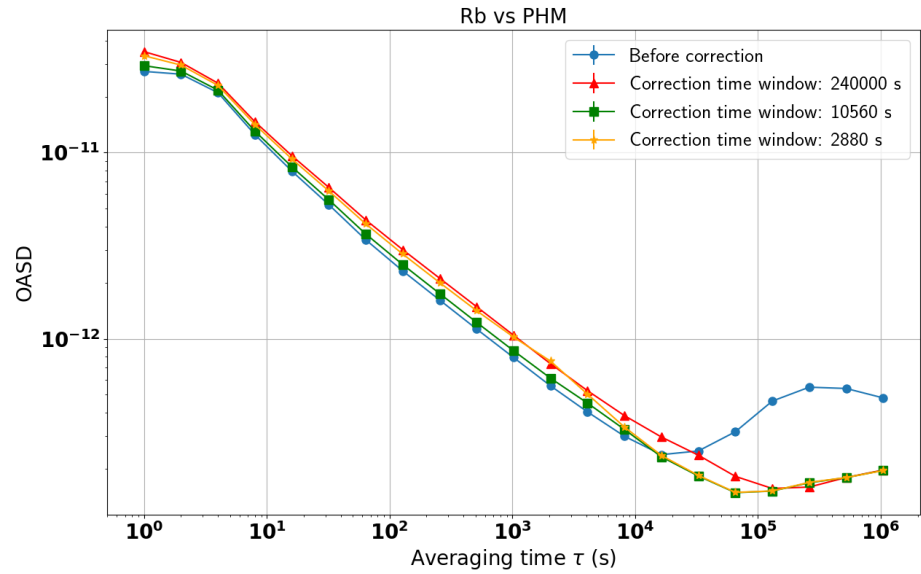


**Figure 11.** Overlapping Allan Standard deviation of the Rb/PHM frequency ratios series after the deterministic drift correction (in blue) and after the correction with a correction time window of 2880 s (orange), 10560 s (green) and 240,000 s (red). The best stability at both short and long averaging times is obtained for the medium time window ( $10560 \approx 3$  hours).

distribution. The blue distribution shows the result for series corrected only for the deterministic drift of the Rubidium clock, by subtracting the expected time distribution of the series caused by this drift. Note that by correcting the deterministic drift, we also partially correct for the frequency random walk such that the OASD decreases with the averaging times for  $\tau > 10^6$  s. In the following, the so-called "uncorrected" distributions are already corrected for this long term drift. The other colors show the results for the series corrected offline, with different width of the correction time window. Here, we use quadratic fits of the Septentrio data (so  $a_k \neq 0$  a priori). The shortest time window (2880 s) corresponds to approximately 3 Septentrio 16 minutes epochs, so 3 points in the Rb vs GPS time residuals distribution. The medium (10560 s) and largest (240,000 s) correspond respectively to 11 and 250 Septentrio data points.

One sees that with the medium time window compared to the two others, we obtain the best stability at all averaging times. At lower averaging times, the performance is very similar to the uncorrected time series. At higher averaging times, the Allan Standard Deviation is much better than the uncorrected time series and is comparable to the one obtained for the shortest correction time window. This illustrates the fact that both the 2880 s and 10560 s windows are able to correct very well the frequency random walk ( $\tau^{1/2}$  component of the ASD) of the uncorrected time series. However, with the shortest correction time window, the short term stability of the time series is degraded compared to the uncorrected series: the value of the ASD at 1 s increases by a factor  $\sim 1.5$ . In this scenario, the corrected Rubidium time signal gets very close to GPS Time which is known to have a higher phase White Noise. Finally, the longest correction time window leads to a similar stability as the shortest one at long term and even poorer stability at  $\tau \in [10^4, 10^5]$  s.

Figure 12 shows the Rubidium time residuals distribution after the offline correction against GPS Time. The shorter the correction time window, the better. However, with the medium length time window, we still get time residuals lower than 5 ns over the whole data-taking period, which is well below the requirements of HK. With the longest correction time window, jumps of a few tens of nanoseconds are introduced in the time distribution of the time residuals. This explains the overall higher ASD: the stability of the signal is limited by those jumps. These jumps can be understood by looking at the fit of the time residuals

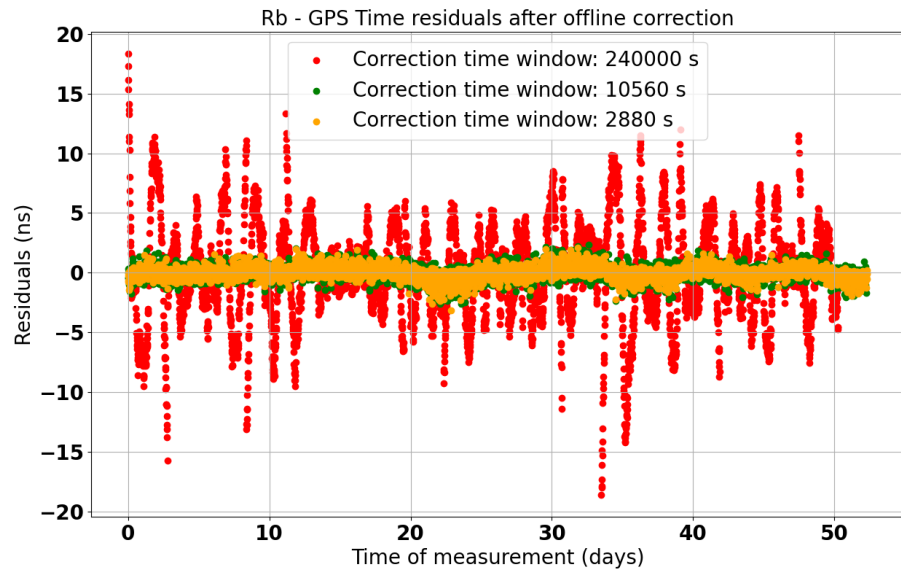


**Figure 12.** Time distribution of the time residuals between the Rubidium clock and GPS Time after the offline correction. Three different correction time windows have been tested: 2800 s (orange), 10560 s (green) and 240,000 s (red). These residuals can be compared to the residuals before correction that were shown in Figure 10.

distribution against GPS in this scenario in Figure 13. The time scale of the variations in the data to fit is too small compared to the 240,000 s time window. In consequence, the fitted tendency from one piece to another is very different and the fitted piece-wise polynomial is not continuous.

With the offline version of the corrections, we thus obtain a very good synchronisation to GPS Time at the level of a few nanoseconds with the 10560 s time window. However, this version of the correction cannot be applied in real time. In the following paragraphs, we show the results for the online version of the correction that can be applied to correct in real time the time stamps of events in physics experiments.

### 3.2. Online correction

Figure 14 shows the Allan standard deviation of the uncorrected (blue) and online corrected (other colors) Rubidium/PHM frequency ratios series. The same three time window intervals as in the offline correction scenario are considered. The top panel shows the results using quadratic fits of the Septentrio data and the bottom panel shows the results with linear fits. For the shortest and medium correction time windows, the linear fits lead to better performance with a lower ASD at low averaging times. At 1 s, the ASD with the shortest (medium) correction time window is reduced by a factor 4 (resp.  $\sim 1.5$ ).

This behavior is very understandable looking at the number of degrees of freedom (number of data points - number of free parameters) in our fits. For the shortest time windows, the number of degrees of freedom is relatively low (0 and 8) in case of quadratic fits so we risk over-fitting to the past data in order to correct the present data. This number of degrees of freedom is not relevant in the offline correction as the fit is performed on the same data as the correction (the over-fitting is not a problem here). Lowering the number of free parameters is one way of increasing the degrees of freedom hence allowing the fit to better generalize to the present data. Another way to increase the number of degrees of freedom is to increase the number of data points in the fit. For the longest time window, there are 247 degrees of freedom in the quadratic fit so we do not risk over-fitting. On the contrary, in that case, quadratic fits lead to a slightly better correction of the random walk that limits the stability only up to  $\tau \approx 8 \times 10^4$  s whereas with linear fits, it limits the

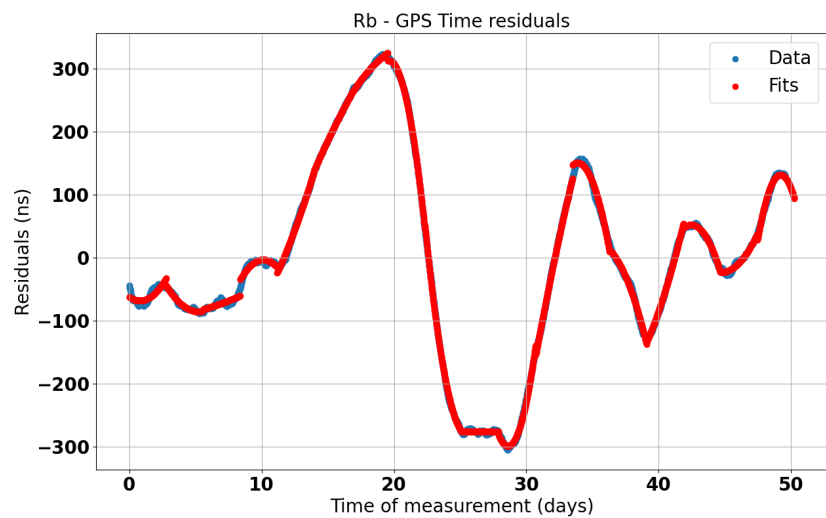


**Figure 13.** Time distribution of the time residuals between the Rubidium clock and GPS Time. The red portions show the results of the polynomial fit over consecutive time windows of 240,000 s. The fit sometimes fail to represent the shorter time scales variations of the measured data. The poor fit quality can then lead to introducing jumps in the corrected time signal.

stability up to  $\approx 2 \times 10^5$  s. Note that the degradation of short term stability because of over-fitting on data from the past is, as expected, also very visible in the OASD of the Rb vs GPS time residuals after correction shown in Figure 15. This plot also illustrates that the corrected signal's stability, compared to GPS Time, is not limited by any frequency random walk at least up to an averaging time or  $2 \times 10^6$  s and correction time window short enough. Indeed, in that case, the OASD keeps decreasing with increasing averaging time.

Regarding the stability of the corrected Rubidium clock, using linear fits, the conclusions are the same as for the offline correction. The lower Allan Standard deviation, for all averaging times, is achieved with the medium width correction time window. With the shortest time window, the short term stability is degraded, whereas it is the long term stability that is degraded (compared to the other corrected scenarios) with the longest correction time window. Note that, contrary to the offline correction, the online correction with very long time windows does not deteriorate the short term stability of the signal. This is due to the use of "overlapping" windows of Rb vs GPS data. Between two consecutive fits, there is only one data point out of the 250 used that changes (the oldest one from the previous fit is replaced by the newest point). The fit parameters cannot change too abruptly from one fit to another so the resulting distributions are smooth.

If the correction time window is too wide, we cannot correct as well the frequency random walk of the free running Rubidium: the risk is that the Rubidium time signal locally drifts too far away from the GPS Time. This can be observed in the corrected Rubidium against GPS in Figure 16 where the maximum residual reaches  $\sim 60$  ns (or  $\sim 25$  ns with quadratic fits) with the 240,000 s correction time window. With the 10560 s correction time window, the residuals stay in the  $\pm 5$  ns range. Once again, one can see the reduction of the white noise when using linear instead of quadratic fits for the 2880 s correction time window scenario: the residuals are contained in a  $\pm 5$  ns range with linear fits instead of  $\pm 12$  ns with quadratic fits. Note that with linear fits, the difference of OASD at  $10^5$  s between the longest time window and the others is only of a factor 2.3, and the difference between the shorter time windows and the uncorrected OASD is only a factor 3. Such small differences have a significant impact in terms of synchronisation to GPS Time. Before correction, as the reader saw in Figure 10, the free running Rubidium clock can drift by around 100 ns in 10 days which means that HK's requirement for the synchronisation with UTC is not met. After online correction with the longest time window tested, the corrected

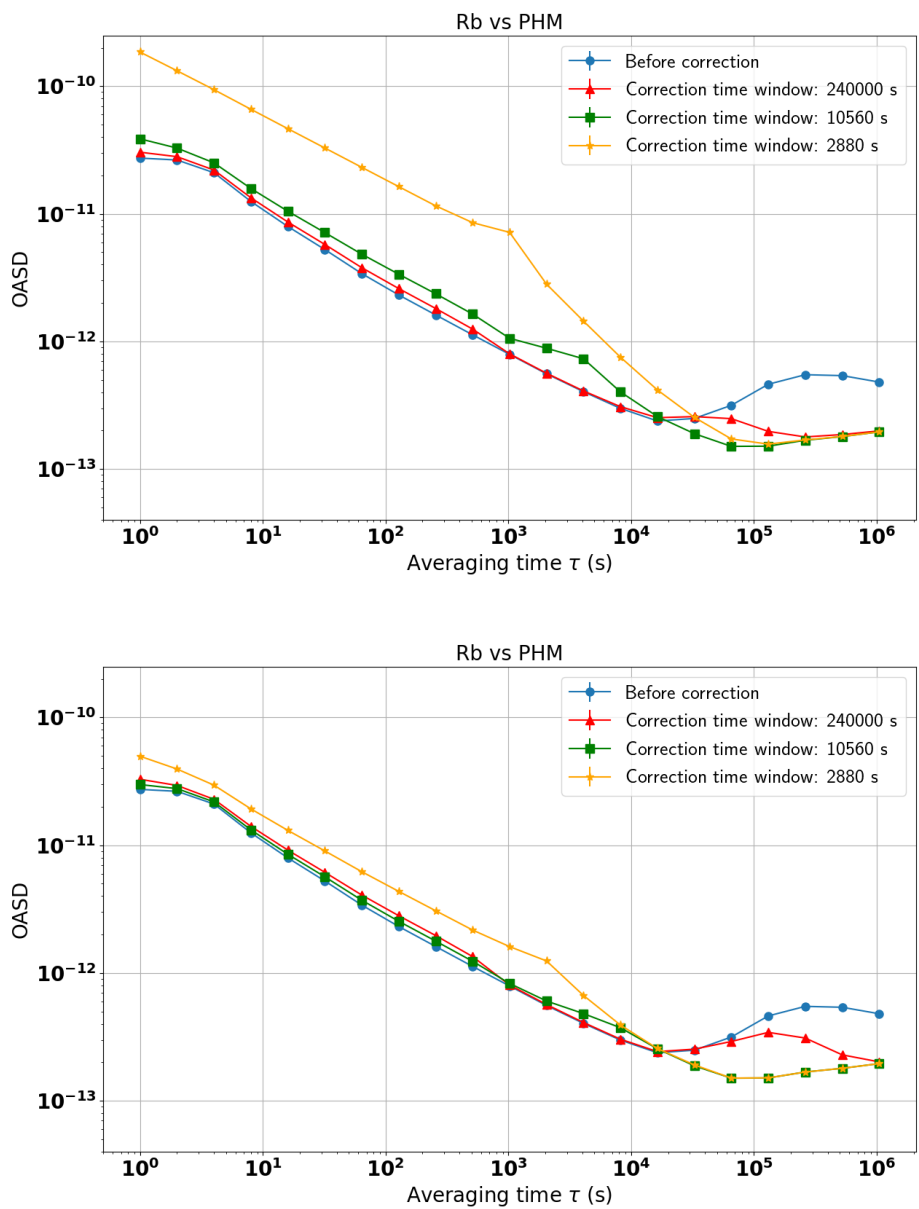


**Figure 14.** Overlapping Allan Standard deviation of the Rb/PHM frequency ratios series after the deterministic drift correction (in blue) and after the online correction with a correction time window of 2880 s (orange), 10560 s (green) and 240,000 s (red). The data were fitted with quadratic (top) or linear (bottom) functions of time. A better stability, similar to the offline correction, can be obtained using linear fits.



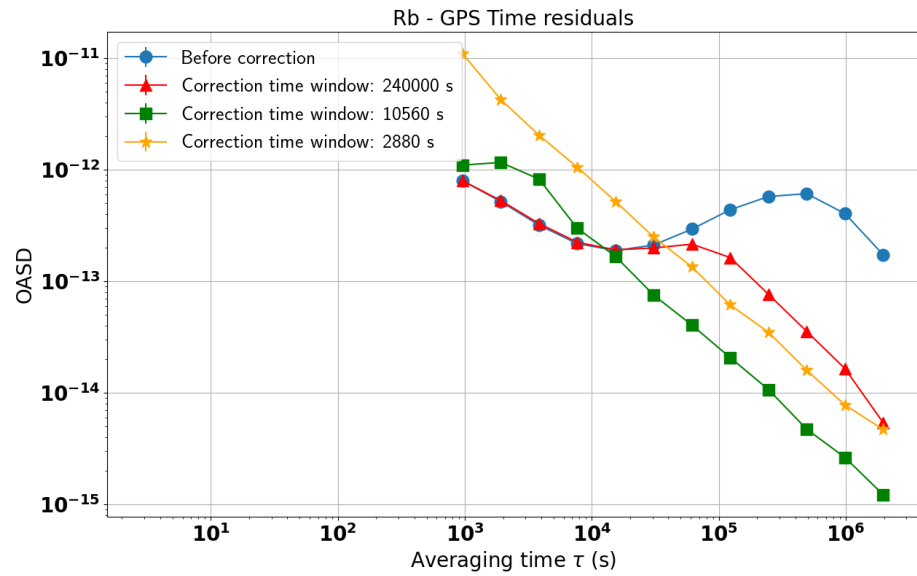


**Figure 15.** Overlapping Allan Standard Deviation of the Rb vs GPS time residuals series after the deterministic drift correction (in blue) and after the online correction with a correction time window of 2880 s (orange), 10560 s (green) and 240,000 s (red). Note that before the deterministic drift correction, the OASD of this signal is the combination of the GPS Time OASD at low  $\tau$  and the Rubidium OASD at high  $\tau$ , i.e: the combination of the blue and orange curves of Figure 2. The deterministic drift correction slightly smooths the residuals so that the OASD becomes generally lower and the frequency drift and random walk at high  $\tau$  disappears, hence the decreasing OASD in the blue curve at very high  $\tau$ . The time residuals were fitted with quadratic functions of time. The increase of OASD at 1 s averaging time with decreasing correction time window is consistent with what is observed in the Rb/PHM frequency ratios series after online correction. The less degrees of freedom in the fit, the more we risk over-fitting on past data and lowering the short term stability of the signal.

Rubidium clock drifts by around 60 ns in a few days because of remaining random walk noise. Even though during the 50 days data-taking period the time residuals with respect to GPS Time does not exceed 100 ns, it is not possible to safely claim that the Rubidium clock drift will not exceed HK's requirement of 100 ns if we use the 240,000 s correction time window. With shorter time windows, this drift seems to be dominated by white noise and is thus contained in a range of a few nanoseconds.

#### 4. Discussion

As advertised before, the advantage of the so-called online correction is that it could be performed in real-time. This is an important feature for applications that necessitate a real-time synchronization with UTC or with another site (like the future HK or DUNE experiments) via a common-view GPS technique [25]. The common-view would be performed with a national laboratory providing a local realization of UTC(k), like e.g. the NICT laboratory in Japan [27], then the conversion to UTC can be performed with the help of the Circular T of the BIMP (Bureau International des Poids et Mesures) [28] at the end of each month. If a reference clock signal is generated with an atomic clock (like the Rubidium clock used here) and sent to a data acquisition system to be propagated to detectors, one could continuously compare this signal to GPS Time using a Septentrio receiver. The correction coefficients  $a$ ,  $b$  and  $c$  calculated from the Septentrio data would need to be sent to the data acquisition system so that it could correct the time stamps in real-time.

Figure 17 shows the standard deviation of the Rb vs GPS time residuals after correction as a function of the correction time window's width. The performance of the offline and

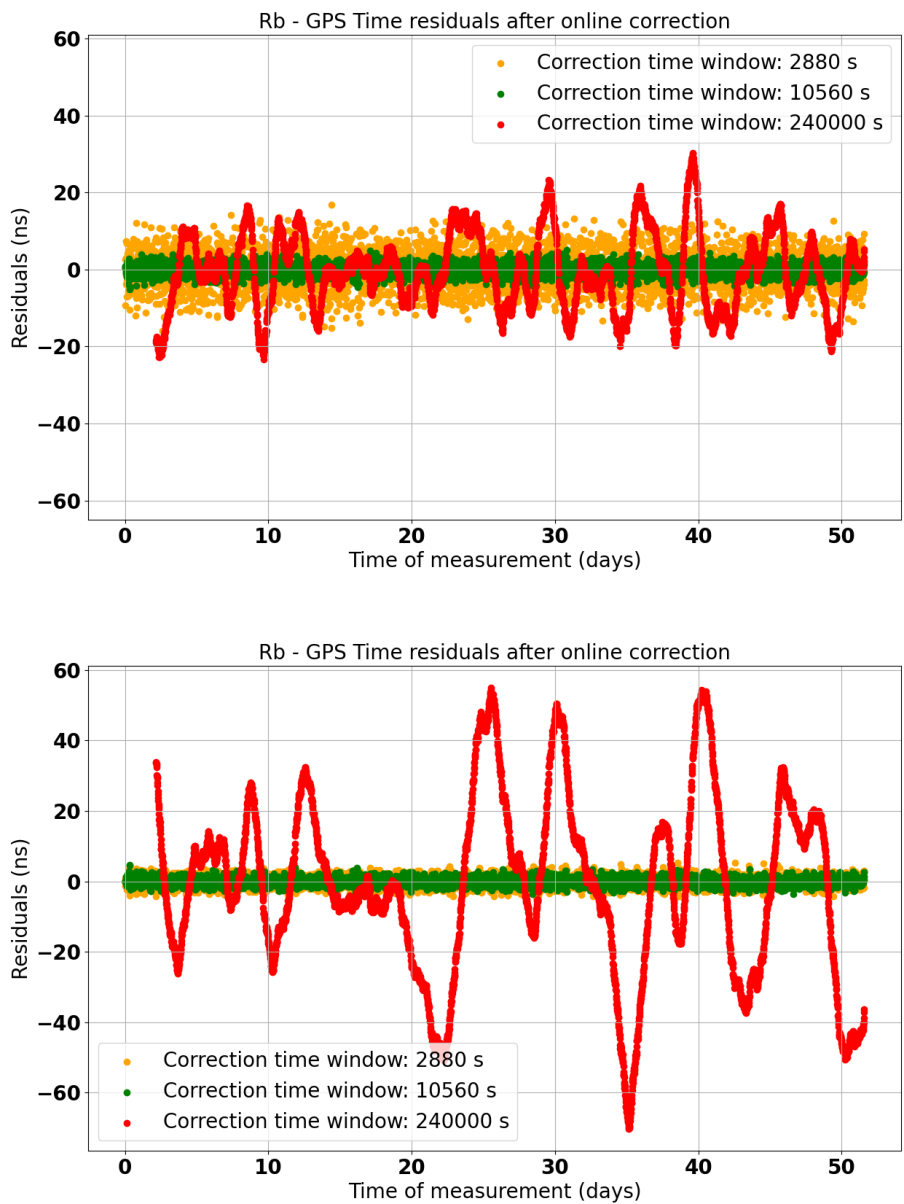


**Figure 16.** Time distribution of the time residuals between the Rubidium clock and GPS Time after the online correction. Each point is corrected using a quadratic (top) or linear (bottom) fit of the 2800 s (orange) or 10560 s (green) or 240,000 s (red) of data points prior to this point. Using linear fits leads to smaller residuals for the shortest time window and bigger ones for the longest time window.

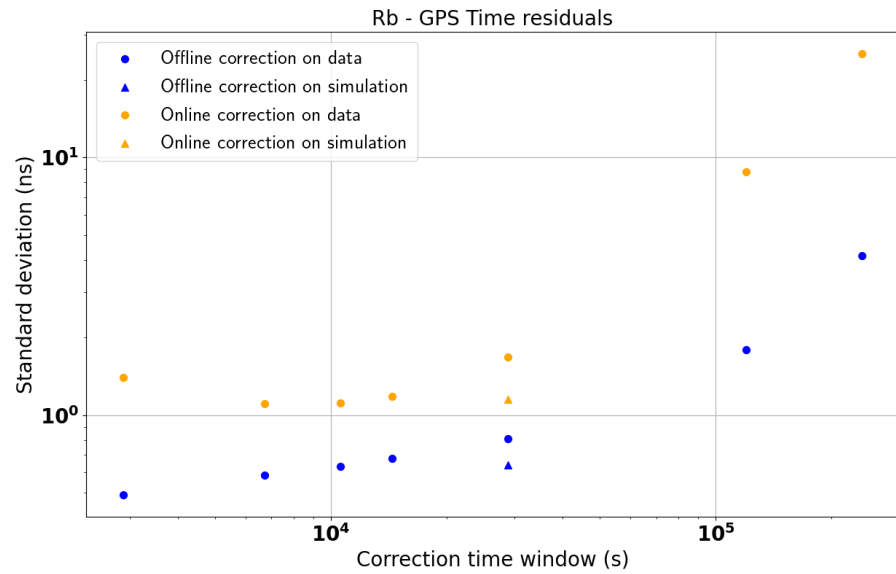


**Figure 17.** Standard deviation of the residuals distributions between the Rb and the GPS 1 PPS signals after the offline (blue) or online (orange) correction as a function of the correction time window. Quadratic fits of the Septentrio data are used for the offline correction whereas linear fits are used for the online correction. The performance on simulated data is also shown for the 10560 s time window with star markers.

online correction on experimental data (colored dots) is compared to the performance we had obtained on simulated data (colored asterisks) with a correction time window of 10560 s. Note that these simulated data were only taking into account white noises and frequency random walk. No additional uncertainty was added to take into account other types of noise (e.g: flicker noise) or experimental conditions (e.g: imperfect calibrations, imperfect PHM time signal). These differences can explain the slightly better performance obtained on simulated data (0.64-1.15 ns at 28,800 s) compared to experimental data (0.81-1.67 ns at 28,800 s) and the fact that the residuals are minimal with a time window of 28,800 s with simulated data and 10,560 s with experimental data. For both corrections, very similar performance of synchronization with GPS Time are obtained for correction time windows below 30,000 s so there is no need to have much shorter windows. This result is consistent with the fact as seen in Figure 2, the stability of the Rubidium signal becomes limited by the frequency random walk for averaging times around  $10^4$  s. It is also for similar averaging time windows that the Rubidium clock stability becomes worse than GPS Time. It was thus expected to find that similar correction time windows or shorter ones would be needed to efficiently correct for the random walk. The offline correction seems to provide a slightly better synchronization to GPS (down to 1 ns) but the precision affordable with the online correction is already more than satisfying (better than 5 ns for correction time windows below 100,000 s) for synchronization between several experimental sites. Indeed, the needed level of synchronization is usually of the order of 100 ns for those applications.

## 5. Conclusions

In this paper, we presented a simple way to use time comparisons to GPS Time to correct the time signal generated by a free running Rubidium clock to synchronize it close to UTC while preserving its short term stability and correcting the long term frequency random walk. This method has the advantage of using relatively cheap instruments and to be applicable online for a real-time synchronization as well as to be robust against GPS signal reception failures. The online method could be applied for the real-time synchronization between several experimental sites in physics experiments.

This method consists in fitting the GPS Time vs Rb measured by a GPS receiver with a piece-wise polynomial function of time and in subtracting the result to the generated time stamps. The method was first designed and validated with simulated signals before assessing its performance on data. We evaluated the performance of this correction by quantifying the stability of the clock signal before and after the correction using the Allan Standard Deviation. We showed that the optimal length of the time window for the fit of the GPS Time vs Rb seats around 10,000 seconds, corresponding to  $\sim 10$  data points from the receiver. This time window allowed to maintain the best possible short term stability of our generated signal while correcting the drifts caused by the frequency random walk. After correction with this time window, the GPS Time vs Rb stay within a window of  $\pm 3.5$  ns ( $\pm 5$  ns) for the offline (resp. online) correction during the whole period of  $\sim 50$  days of measurement. This performance largely meets the usual requirements for physics experiments like Hyper-Kamiokande. Note that we do not expect the performance of the correction to be heavily degraded by isolated missing or outlier measurement from the receiver. However, this correction requires a constant monitoring of the Rubidium time signal with a GNSS receiver (or other reference that can be linked to UTC). One should thus make sure that such a reference is available in the long term and that there is no possibility to loose it for long periods (e.g.: several hours).

**Author Contributions:** For research articles with several authors, a short paragraph specifying their individual contributions must be provided. The following statements should be used “Conceptualization, X.X. and Y.Y.; methodology, X.X.; software, X.X.; validation, X.X., Y.Y. and Z.Z.; formal analysis, X.X.; investigation, X.X.; resources, X.X.; data curation, X.X.; writing—original draft preparation, X.X.; writing—review and editing, X.X.; visualization, X.X.; supervision, X.X.; project administration, X.X.; funding acquisition, Y.Y. All authors have read and agreed to the published version of the manuscript.”, please turn to the [CRediT taxonomy](#) for the term explanation. Authorship must be limited to those who have contributed substantially to the work reported.

**Funding:** Please add: “This research received no external funding” or “This research was funded by NAME OF FUNDER grant number XXX.” and and “The APC was funded by XXX”. Check carefully that the details given are accurate and use the standard spelling of funding agency names at <https://search.crossref.org/funding>, any errors may affect your future funding.

**Institutional Review Board Statement:** In this section, you should add the Institutional Review Board Statement and approval number, if relevant to your study. You might choose to exclude this statement if the study did not require ethical approval. Please note that the Editorial Office might ask you for further information. Please add “The study was conducted in accordance with the Declaration of Helsinki, and approved by the Institutional Review Board (or Ethics Committee) of NAME OF INSTITUTE (protocol code XXX and date of approval).” for studies involving humans. OR “The animal study protocol was approved by the Institutional Review Board (or Ethics Committee) of NAME OF INSTITUTE (protocol code XXX and date of approval).” for studies involving animals. OR “Ethical review and approval were waived for this study due to REASON (please provide a detailed justification).” OR “Not applicable” for studies not involving humans or animals.

**Data Availability Statement:** We encourage all authors of articles published in MDPI journals to share their research data. In this section, please provide details regarding where data supporting reported results can be found, including links to publicly archived datasets analyzed or generated during the study. Where no new data were created, or where data is unavailable due to privacy or ethical restrictions, a statement is still required. Suggested Data Availability Statements are available in section “MDPI Research Data Policies” at <https://www.mdpi.com/ethics>.

**Acknowledgments:** In this section you can acknowledge any support given which is not covered by the author contribution or funding sections. This may include administrative and technical support, or donations in kind (e.g., materials used for experiments).

**Conflicts of Interest:** Declare conflicts of interest or state “The authors declare no conflicts of interest.” Authors must identify and declare any personal circumstances or interest that may be perceived as inappropriately influencing the representation or interpretation of reported research results. Any role of the funders in the design of the study; in the collection, analyses or interpretation of data; in the

writing of the manuscript; or in the decision to publish the results must be declared in this section. If there is no role, please state "The funders had no role in the design of the study; in the collection, analyses, or interpretation of data; in the writing of the manuscript; or in the decision to publish the results".

### Abbreviations

The following abbreviations are used in this manuscript:

MDPI	Multidisciplinary Digital Publishing Institute
ASD	Allan Standard Deviation
OASD	Overlapping Allan Standard Deviation
Rb	Rubidium clock
PHM	Passive Hydrogen Maser
GPS	Global Positioning System
UTC	Universal Time Coordinated
GPS	Global Navigation Satellite Systems
HK	Hyper-Kamiokande
DUNE	Deep Underground Neutrino Experiment
PPS	Pulse Per Second
WR	White Rabbit

### Appendix A

#### References

1. K. Abe *et al.*, Hyper-Kamiokande Proto-Collaboration, Hyper-Kamiokande Design Report. *arXiv:1805.04163*, 2018. 543
2. M. Guler *et al.*, OPERA: An appearance experiment to search for  $\nu/\mu \leftrightarrow \nu/\tau$  oscillations in the CNGS beam. Experimental proposal, CERN-SPSC-2000-028; 544
3. K. Abe *et al.*, T2K Collaboration, The T2K Experiment, Nucl. Instrum. Meth. A **659** (2011), 106-135, doi:10.1016/j.nima.2011.06.067, [arXiv:1106.1238 [physics.ins-det]]. 545
4. D.S. Ayres *et al.*, The NOvA Technical Design Report, (2007), doi:10.2172/935497 546
5. B. Abi *et al.*, Deep Underground Neutrino Experiment (DUNE), Far Detector Technical Design Report, Volume I: Introduction to DUNE, *arXiv:2002.02967*, 2020. 547
6. Mészáros, P., Fox, D.B., Hanna, C. et al. Multi-messenger astrophysics. *Nat Rev Phys* **1**, 585–599 (2019). <https://doi.org/10.1038/s42254-019-0101-z> 548
7. The Supernova Early Warning System web page. <https://snews2.org/>. 549
8. K. Abe *et al.*, T2K collaboration, Upper bound on neutrino mass based on T2K neutrino timing measurements, *Physical Review D* (93), 2016, DOI: 10.1103/PhysRevD.93.012006, <https://arxiv.org/abs/1502.06605> 550
9. Y. Fukuda *et al.*, Super-Kamiokande collaboration, The Super-Kamiokande detector, *Nucl.Instrum.Meth.A* **501** (2003) 418, [https://doi.org/10.1016/S0168-9002\(03\)00425-X](https://doi.org/10.1016/S0168-9002(03)00425-X). 551
10. Mellet, L.; Guigue, M.; Popov, B.; Russo, S.; Voisin, V., on behalf of the Hyper-Kamiokande Collaboration. Development of a Clock Generation and Time Distribution System for Hyper-Kamiokande. *Phys. Sci. Forum* **2023**, *8*, 72. <https://doi.org/10.3390/psf2023008072>. 552
11. Lombardi, M. *Fundamentals of Time and Frequency*. In *The Mechatronics Handbook*; CRC Press: Boca Raton, FL, USA, 2002; ISBN 978-0-8493-6358-0. 553
12. Giulia Brunetti. Neutrino velocity measurement with the OPERA experiment in the CNGS beam. Other [cond-mat.other]. Université Claude Bernard - Lyon I; Università degli studi (Bologna, Italie), 2011. English. (NNT : 2011LYO10088). (tel-00843100) 554
13. Howe, D.A.; Allan, D.U.; Barnes, J.A. Properties of signal sources and measurement methods. In *Proceedings of the Thirty Fifth Annual Frequency Control Symposium*, Philadelphia, USA, 27-29 May 1981. 555
14. Serrano, J. et al., The White Rabbit project, 2013. <https://cds.cern.ch/record/1743073> 556
15. Daniluk, G, White Rabbit calibration procedure (version 1.1), 2015. [https://white-rabbit.web.cern.ch/documents/WR\\_Calibration-v1.1-20151109.pdf](https://white-rabbit.web.cern.ch/documents/WR_Calibration-v1.1-20151109.pdf) 557
16. E. Cantin et al., "REFIMEVE Fiber Network for Time and Frequency Dissemination and Applications," 2023 Joint Conference of the European Frequency and Time Forum and IEEE International Frequency Control Symposium (EFTF/IFCS), Toyama, Japan, 2023, pp. 1-4, doi: 10.1109/EFTF/IFCS57587.2023.10272084. 558
17. C. B. Lim et al., "Extension of REFIMEVE with a White Rabbit Network," 2023 Joint Conference of the European Frequency and Time Forum and IEEE International Frequency Control Symposium (EFTF/IFCS), Toyama, Japan, 2023, pp. 1-4, doi: 10.1109/EFTF/IFCS57587.2023.10272069. 559
18. Defraigne, P.; Petit, G. CGGTTS-Version 2E: an extended standard for GPS Time Transfer, *Metrologia* (52), IOP Publishing, 2015, DOI: 10.1088/0026-1394/52/6/G1 560

19. Mellet, L. From T2K to Hyper-Kamiokande : neutrino oscillation analysis and preparation of the time synchronization system. 2023, (NNT : 2023SORUS297). (tel-04284182) 588
20. Plumb, John et al. Absolute calibration of a geodetic time transfer system. *Ultrasonics, Ferroelectrics and Frequency Control, IEEE Transactions on* (2005) **52**, 1904-1911 doi = 10.1109/TUFFC.2005.1561658 589
21. J. A. Barnes et al., "Characterization of Frequency Stability," in *IEEE Transactions on Instrumentation and Measurement*, vol. IM-20, no. 2, pp. 105-120, May 1971, doi: 10.1109/TIM.1971.5570702. 590
22. T. J. Witt, "Using the Allan variance and power spectral density to characterize DC nanovoltmeters," in *IEEE Transactions on Instrumentation and Measurement*, vol. 50, no. 2, pp. 445-448, April 2001, doi: 10.1109/19.918162. 591
23. D. W. Allan, "Statistics of atomic frequency standards," in *Proceedings of the IEEE*, vol. 54, no. 2, pp. 221-230, Feb. 1966, doi: 10.1109/PROC.1966.4634. 592
24. W.J. Riley. Handbook of frequency stability analysis. NIST Special publication 1065. July 2008. 593
25. Weiss, M.A.; Petit, G.; Jiang, Z. A comparison of GPS common-view time transfer to all-in-view. In *Proceedings of the IEEE International Frequency Control Symposium and Exposition, 2005*. 594
26. <https://webapp.csrscs.nrcan-rncan.gc.ca/geod/tools-outils/ppp.php> 595
27. The National Institute of Information and Communications Technology (NICT), Japan. <https://www.nict.go.jp/en/> 596
28. <https://www.bipm.org/en/time-ftp/circular-t> 597
29. G. D. Rovera et al., "UTC(OP) based on LNE-SYRTE atomic fountain primary frequency standards", *Metrologia* 53 S81, 2016. 598
30. G. D. Rovera et al., "Link calibration against receiver calibration time transfer uncertainty when using the Global Positioning System", *Metrologia* 51.5 476490, 2014. 599

**Disclaimer/Publisher's Note:** The statements, opinions and data contained in all publications are solely those of the individual author(s) and contributor(s) and not of MDPI and/or the editor(s). MDPI and/or the editor(s) disclaim responsibility for any injury to people or property resulting from any ideas, methods, instructions or products referred to in the content. 600